Optimized light source spectral power distribution for RGB camera based spectral reflectance recovery

LIXIA WANG,[1,2] **ADITYA SOLE,**[2] **JON YNGVE HARDEBERG,**[2,4] **AND XIAOXIA WAN**[1,3,5]

[1]*School of Printing and Packaging, Wuhan University, Wuhan 430079, China*
[2]*Department of Computer Science, Faculty of Information Technology and Electrical Engineering, Norwegian University of Science and Technology, 2815 Gjøvik, Norway*
[3]*Hubei Province Engineering Technical Center for Digitization and Virtual Reproduction of Color Information of Cultural Relics, Wuhan 430079, China*
[4]*jon.hardeberg@ntnu.no*
[5]*wan@whu.edu.cn*

Abstract: The accuracy of recovered spectra from camera responses mainly depends on the spectral estimation algorithm used, the camera and filters selected, and the light source used to illuminate the object. We present and compare different light source spectrum optimization methods together with different spectral estimation algorithms applied to reflectance recovery. These optimization methods include the Monte Carlo (MC) method, particle swarm optimization (PSO) and multi-population genetic algorithm (MPGA). Optimized SPDs are compared with D65, D50 A and three LED light sources in simulation and reality. Results obtained show us that MPGA has superior performance, and optimized light source spectra along with better spectral estimation algorithm can provide a more accurate spectral reflectance estimation of an object surface. Meanwhile, it is found that camera spectral sensitivities weighted by optimized SPDs tend to be mutually orthogonal.

1. Introduction

Spectral reflectance property of a material tells how strongly the material reflects light incident on it and can be defined as the material's 'fingerprint'. It has been widely used in various application domains such as cultural heritage [1,2], medical diagnosis [3], remote sensing [4], and color measurement and color quality control in paint, plastic, inks, print and textile industries [5,6]. Spectral reflectance acquisition with enough spatial accuracy, however, can be complicated. Different methods that are used to capture spectral reflectance of an object surface with a high spatial accuracy are presented and described in [7–17]. The approaches described in [7–9] are direct and capable of providing accurate spectral reflectance with a reasonable sampling interval in wavelength. The methods presented in [10–17] are indirect and therefore less accurate as they obtain an estimation of the spectral reflectance from a reduced number of channel responses. Methods with a direct approach generally have a low acquisition speed, complex hardware assembly, and high cost while the indirect methods can be less expensive and easier to implement thus in many cases are more preferred compared to the direct methods.

In recent years, research on spectral reflectance estimation has been focused mainly on spectral estimation algorithms, filter selection, and light source selection. In addition to the traditional spectral reflectance estimation techniques such as pseudo-inverse estimation, matrix R, and principal component analysis, many researchers have proposed various improved methods like general regularization framework, regularized local linear model, and sequential weighted nonlinear regression model [12–17] to name a few. For designing or selecting appropriate filters

different algorithms like equi-spacing of filter central wavelengths, exhaustive search, and genetic algorithm have been proposed [18,19]. Apart from spectral estimation algorithm and filter selection, design and selection of light source to capture object surface reflectance also play a vital role in spectral imaging [10,11,20,21]. Tominaga *et al.* [10] developed a multispectral imaging system that synchronized a programmable light source and a high-speed monochrome camera. Shrestha *et al.* [20] employed the simple pseudo-inverse method and exhaustive search to select the optimal 3 light-emitting diodes (LEDs) from 19 LEDs to build a multispectral imaging system. Similarly, Zhang *et al.* [11] also utilized the pseudo-inverse method based on XYZ values instead, selected 3 illuminants from 8 CIE illuminants and 3 LEDs to estimate spectral reflectance. Zhang *et al.* [21] optimized many combinations of peak wavelengths, the full width at half maximums (FWHMs) of projector spectral power distributions (SPDs) and camera responsivities to derive simulated system functions.

However, these methods selected an optimal subset from a certain number of specific light sources or optimized unreal simulated SPDs. Additionally, with the selected light sources, the above methods tend to use simple pseudo-inverse techniques to estimate spectral reflectance. This results in ignoring the influence of estimation algorithms on the optimized light source and accuracy.

With the above in mind, in this paper, we demonstrate using an optimized SPD together with an appropriate spectral estimation algorithm to improve the accuracy in estimating spectral reflectance of an object using RGB camera response. The SPD of the light source is optimized using various optimization techniques such as Monte Carlo (MC) method, particle swarm optimization (PSO) and multi-population genetic algorithm (MPGA).

A commercially available LED-based spectral tunable light source LEDCube, manufactured by Thouslite [22], consisting of 11 different LEDs, is used as a light source to illuminate object surface. Various optimization methods together with different spectral estimation algorithms are used to optimize light source SPDs and recover spectral reflectance. In addition, we investigate the influence of RGB camera sensitivity and target samples on the optimized SPDs of light source. The main contributions of this paper are summarized as follows:

(1) The use of a light source with optimized SPD instead of using standard light source to recover spectral reflectance using estimation algorithm and RGB camera responses.

(2) Various optimization techniques instead of the exhaustive search method to optimize the 11 different LEDs of the tunable light source.

(3) Selecting an appropriate spectral estimation algorithm together with the optimal light source to estimate spectral reflectance.

(4) Influences of camera spectral sensitivities and target samples on optimized SPD are investigated, and correlation between optimized SPD and camera spectral sensitivities is found.

2. Background and related work

The responses of a camera with three channels are dependent on the light source SPD $L(\lambda)$, the reflectance $r(\lambda)$ of the captured object, the camera sensitivity function $c_k(\lambda)$ and system noise n_k. The camera response u_k can be written in a simple imaging model [23],

$$u_k = \int_\omega L(\lambda)r(\lambda)c_k(\lambda) + n_k, k \in \{R, G, B\}, \tag{1}$$

where ω denotes the visible spectrum. Equation (1) can be written as a matrix equation:

$$\mathbf{u} = \mathbf{Mr} + \mathbf{n}, \tag{2}$$

where **u** denotes the response vector of three channels, **M** represents the spectral responsivity including the light source SPD and the camera spectral sensitivities, **r** denotes the spectral reflectance, and **n** is the noise term.

Many methods have been proposed to estimate spectral information from camera responses. In general, these methods fall into three branches: traditional, machine learning, and deep learning methods. Traditional methods are simple and easy to perform [11–17,24–28], but machine learning and deep learning methods either has low recovery accuracy [29] or require a huge size of training set [30,31]. In this work, traditional methods are mainly taken into account. These methods include classical methods like wiener estimation, principal component analysis, pseudo-inverse estimation, their various modified versions, and some other methods with no training set required. Compared to wiener estimation with a certain complexity due to camera sensitivity characterization required, generalized methods based on statistics are more concerned. Ayala *et al.* [24] divided reflectance spectra data into ten subgroups according to the hue similarity of samples and calculated the first three eigenvectors for each hue. Heikkinen *et al.* [12] utilized a general regularization framework for robust spectral estimation. Heikkinen *et al.* [25] and Eckhard *et al.* [14] proposed different kernel-based regression models to recover reflectance and obtained a relatively high accuracy. Amiri and Fairchild [15] utilized weighted nonlinear regression model to reduce spectral errors between recovered and real spectra. In addition to the above global solutions, some researchers found that recovery performance could be improved by adaptively selecting local training samples. Zhang *et al.* [13] recovered reflectance by a linear combination of *k* reflectances from training set that have similar camera responses to target sample. Liang *et al.* [16] developed a local Gaussian weighted linear regression model for spectral estimation from raw camera responses. Wang *et al.* [17] used colorimetric and spectral errors between training set and target set successively to adaptively select training samples and constructed two nonlinear regression models for spectral recovery. Moreover, there are some other traditional methods starting from various premises. Morovic and Finlayson [26] proposed an elegant solution to estimate reflectance by calculating metamer set and chose a member from this set based on three different assumptions that all reflectances were equally likely, followed a normal probability distribution, or were smooth. Li and Luo [27] used numerical optimization techniques with explicit inequality constraints to recover the smoothest reflectance. Burns [28] found the smoothest reflectance in metamer set by using a hyperbolic tangent transformation to limit reflectance between 0 and 1, and recovered reflectance with a higher accuracy than Li and Luo.

3.　Light source SPD optimization method

The optimal light source when estimating the spectral reflectance of an object surface is defined as the light source resulting in the most accurate spectral reflectance estimation of the target samples. We used a commercially available LED-based spectrally tunable light source consisting of 11 different LEDs that can generate different SPDs by adjusting the drive current of each LED. According to the SPD superposition model [32], the synthesized SPD can be obtained as

$$L(\lambda) = \sum \chi_i L_i(\lambda), \tag{3}$$

where $L(\lambda)$, $L_i(\lambda)$ and χ_i are the final SPD of the light source, the SPD of the *i*th channel when the drive current is equal to the rated current, and the weight coefficient of the *i*th channel, respectively. The weight coefficient for each LED can be adjusted in the range of 0-100% at an interval of 0.1% thus generating the possibility to emit approximately 1.001×10^{33} different kinds of SPDs. Selecting the optimal SPD therefore can be very difficult and impractical using an exhaustive search algorithm. To address this discrete constrained optimization issue, Monte Carlo (MC) method and evolutionary algorithm such as particle swarm optimization (PSO) and

multi-population genetic algorithm (MPGA) based optimization could be used, in particular, in this situation where 11 LED channels need to be optimized.

3.1. Monte Carlo (MC) method

As a sampling-based stochastic optimization method, MC has been widely used to solve optimization problems due to its simplicity and versatility since its introduction more than half a century ago [33]. A generic way of describing it is to construct an approximating problem. Consider a family $\{g_N(\cdot)\}$ of random approximations of the function $g(\cdot)$. χ is the decision vector which must satisfy the set of deterministic constraint X. $\chi^1, \cdots, \chi^N$ are samples from the distribution of ξ. Given the family of estimators $g_N(\chi)$, the corresponding approximating program as Eq. (4) can be constructed.

$$\min_{\chi \in X} g_N(\chi) \tag{4}$$

To adapt the MC method to our application where every element of χ is between 0 and 100% and sampled with steps of 0.1%, the following algorithm is conducted:

Algorithm 1.

(1) Choose an initial objective function value g_0, and let the iteration number $\tau = 1$.

(2) Generate an initial uniformly distributed pseudo - random integer vector χ with 11 elements in the range of [0, 1000].

(3) Every element in the vector is divided by 1000 to be scaled to [0,1]. Then, by Eq. (3), a synthesized SPD can be constructed.

(4) Compute simulated camera responses by Eq. (2).

(5) Based on camera responses and spectral estimation algorithm, reflectance of each testing sample is estimated. Then, for testing set, mean relative absolute error (MRAE), which was chosen as the ranking criterion in NTIRE 2018 and NTIRE 2020 challenge on spectral reconstruction [30,31], is calculated as Eq. (5). Therefore, the objective function of this iteration $g_\tau = MRAE$.

$$MRAE = \frac{1}{N} \sum_{i=1}^{N} (|\hat{\mathbf{r}}_i - \mathbf{r}_i|/\mathbf{r}_i), \tag{5}$$

where $\hat{\mathbf{r}}_i$ and $\mathbf{r}_i$ denote the estimated and actual spectral reflectance of the ith target sample, respectively, and N is the number of target samples.

(6) Check the solution. If $g_\tau < g_0$, set $g_0 = g_\tau$.

(7) Check whether the iteration arrives at the maximum iteration; if not satisfied, set $\tau = \tau + 1$, and loop to step (2). In this work, to be fair, the maximum iteration is set to 3000 to make the optimization time equal to that in the following multi-population genetic algorithm, which converges more slowly than particle swarm optimization.

3.2. Particle swarm optimization (PSO)

PSO is a population-based stochastic optimization algorithm motivated by intelligent collective behavior of flocks of birds and schools of fish. Each particle represents a potential solution and has a position denoted by a position vector ς_i. A swarm of particles moves through the problem space, with the moving velocity of each particle represented by a velocity vector $\mathbf{v}_i$. Each particle keeps track of its coordinate $\mathbf{p}_i$ and fitness value $pbest_i$ in the problem space which denotes the best solution (fitness) it has achieved so far. The best position and fitness value

among all the particles obtained so far in the population are $\mathbf{p}_g$ and $pbest_g$. The generic process for implementing the PSO is as follows [34]:

   Algorithm 2.

   (1) Initialize a population of particles with random positions and velocities on d dimensions in the problem space.

   (2) For each particle, evaluate the desired optimization fitness function in d variables.

   (3) Compare particle's fitness evaluation with particle's $pbest_i$. If current value is better than $pbest_i$, then set $pbest_i$ equal to the current value, and the $pbest_i$ location $\mathbf{p}_i$ equal to the current location.

   (4) Compare fitness value with the population's previous best value $pbest_g$. If current value is better than $pbest_g$, then set $pbest_g$ equal to the current value, and $\mathbf{p}_g$ equal to the current particle's location.

   (5) At each generation τ, update the velocity and position of the particle according to Eq. (6) and (7), respectively:

$$\mathbf{v}_i(\tau + 1) = \mathbf{v}_i(\tau) + c_1\phi_1(\mathbf{p_i}(\tau) - \varsigma_\mathbf{i}(\tau)) + c_2\phi_2(\mathbf{p}_g(\tau) - \varsigma_\mathbf{i}(\tau)), \tag{6}$$

$$\varsigma_i(\tau + 1) = \varsigma_i(\tau) + \mathbf{v}_i(\tau + 1), \tag{7}$$

   where c_1, known as the 'cognitive' component, represents the personal thinking of each particle to move toward best positions; c_2, known as the 'social' component, represents the collaborative effect of the particles in finding the global best solution; both are suggested to be 2.0 for many applications; and ϕ_1 and ϕ_2 are uniformly distributed random numbers in [0,1].

   (6) Go back to step (2) until it reaches the maximum generation.

   In the light source SPD optimization task, each initialized position of each dimension is in the range [0,1000], and it will be scaled as in MC method to construct synthesized SPD; the number of dimension d equals to 11, and the reciprocal of *MARE* in Eq. (5) works as the fitness function. Particle size equals to 60, and maximum generation equals to 50.

   In the literature, Kennedy and Eberhart [34] have pointed out that a relatively high value of the cognitive component leads to excessive wandering of individuals through the search space, and a relatively high value of the social component may result in a local optimum. Therefore, to enhance the global search ability at the early generation and make the particles converge toward the global optimum at the end, c_1 and c_2 are updated at each generation as follows:

$$\omega_0 = 0.9 - 0.5 \times \tau \div \tau_{\max}, \tag{8}$$

$$c_1 = 1 + w_0, \tag{9}$$

$$c_2 = 2.5 - w_0, \tag{10}$$

where $\tau_{\max}$ denotes the maximum number of generations.

3.3. Multi-population genetic algorithm (MPGA)

GA based optimization algorithm starts with a random generation of solutions. Each solution is indicated by a chromosome, and the fitness value of each chromosome is evaluated. During the search process, the chromosome with a better fitness function value has a greater chance to be transferred to the next generation. Unlike PSO, by the crossover and mutation operators,

GA can avoid a local optimum, but a premature convergence may still occur. To enhance the search capability of GA, MPGA has been employed in many applications [35]. MPGA divides a population into multi-subpopulations to perform parallel evolution and introduces the migration operator to strengthen the relationship between these multi-subpopulations. The general algorithm is:

Algorithm 3.

(1) Generate a population randomly with several sub-populations; and let the number of generations $\tau = 1$.

(2) The fitness of individual is evaluated.

(3) Five genetic operation processes are applied to all the individuals: selection, crossover, mutation, reinsertion and migration.

Selection: with a generation gap *GGAP*, the higher the fitness function value obtained from the fitness function, the higher is the likelihood for the corresponding chromosome to be selected for mating compared to chromosomes with a lower fitness value.

Crossover: a crossover operator is used to exchange genetic information between two parent chromosomes to generate new chromosomes. The crossover operation is not necessarily performed on all strings in the population but is applied with a crossover probability p_c when choosing the pairs for breeding.

Mutation: this process changes the chromosome genetic representation with a mutation probability p_{mu}.

Reinsertion: due to the generation gap in the selection operator, new chromosomes are fewer than those in the old sub-populations and therefore new chromosomes are added to the old sub-populations to maintain their size.

Migration: the chromosomes of low fitness in one subpopulation are replaced with chromosomes of high fitness from another subpopulation with a migration probability p_{mi}.

(4) Loop to step (2) until the number of generations overtakes the maximum generation.

In this work, MPGA based on genetic algorithm toolbox from Chipperfield *et al.* [36] is used to find an optimized SPD using the LED-based spectrally tunable light source. The number of control variables is 11 (controllable LEDs in the tunable light source), so the decision variables *NVAR* = 11 are used. Every variable is denoted by 10 genes (*PRECI* = 10) in a binary row vector as given in Eq. (11)

$$\mathbf{O}_i = [1\ 0\ 0\ 1\ 0\ 1\ 0\ 1\ 0\ 0]. \tag{11}$$

With this we have a total of 110 (*PRECI* × *NVAR*) genes, which contain the adjustment information for the 11 LED channels in the tunable light source. This problem may be mapped onto the chromosome structure in the following way:

$$\mathbf{O} = [\mathbf{O}_1\ \mathbf{O}_2\ \mathbf{O}_3\ \cdots\ \mathbf{O}_{11}]. \tag{12}$$

Before the fitness of individual is evaluated, the chromosomes are converted into real values in the range [0, 100%] using an arithmetic scaling since binary coding is used [36]. Then, the reciprocal of *MARE* in Eq. (5) is used as the fitness function.

Based on results of several preliminary runs, the parameters are set as follows: subpopulation size *SUBPOP* = 6, chromosome size in each subpopulation *NIND* = 10, generation gap *GGAP* = 0.95, crossover probability p_c = 0.8, mutation probability p_{mu} = 0.01, migration probability p_{mi} = 0.2, and maximum generation $\tau_{\max}$ = 150.

4. Experiments

Using the above SPD optimization methods along with nine spectral estimation models including pseudo-inverse estimation (PI), regularized least squares (RLS) [12], regularized local linear model (RLLM) [13], radial basis function network (RBF) [29], kernel based model (Kernel) [14], weighted nonlinear regression model (WNR) [15], local-weighted linear regression model (LLR) [16], smoothest reflectance reconstruction (SRR) [28] and sequential weighted nonlinear regression (SWNR) [17], the spectra of light source were optimized, and experimentally tested in this section. The flowchart of SPD optimization experiments is illustrated in Fig. 1.
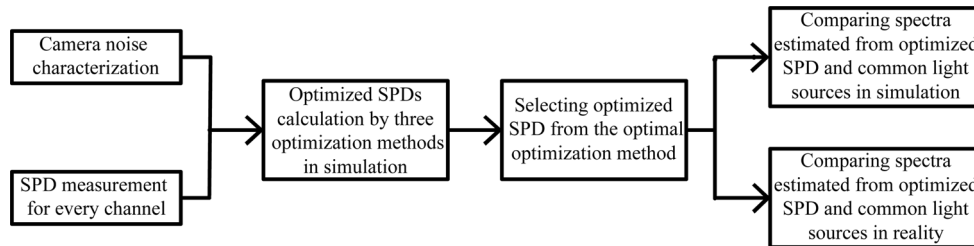

Fig. 1. The flowchart of SPD optimization experiments.

4.1. Camera noise and LED SPD characterization

As can be seen for Fig. 1, firstly, camera noise level and LED SPD of every channel are characterized to simulate camera responses accurately. Figure 2(a) shows the spectral sensitivities of the Nikon D200 camera used in this paper. These camera sensitivities were estimated using measurements from a monochromator and a tele-spectroradiometer [37]. The variance of the noise of this camera was expressed in a Poisson-Gaussian image noise model [38]:

$$\varphi^2 = \alpha u + \sigma^2, \tag{13}$$

where α, u and σ are the Poisson noise parameter, the camera response and the standard deviation of the Gaussian noise, respectively. Then, the X-Rite ColorChecker SG target was captured by this camera, and the above linear model was fitted using the computation method in [39]. For this Nikon D200, $\alpha = 0.0220$, $\sigma^2 = 0.2068$ when raw camera responses were scaled to be in the range of [0, 255].
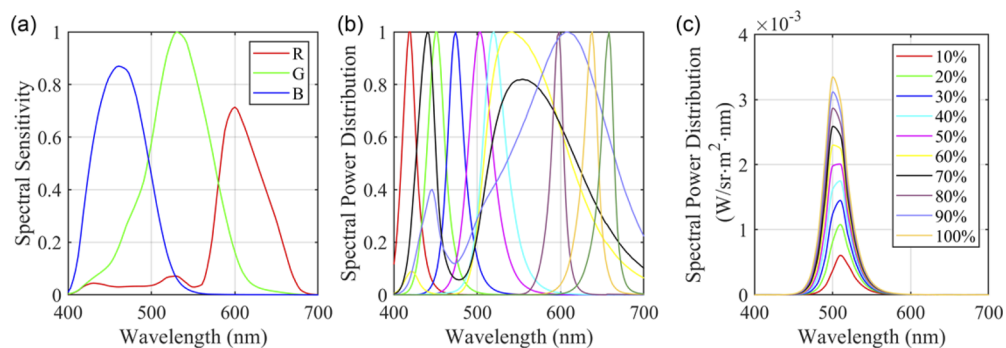
Fig. 2. (a) The spectral sensitivities of Nikon D200, (b) the relative spectral power distributions of 11 channels of the spectrally tunable LED, and (c) the absolute spectral power distributions of the 4th channel of the LED for 10 weight coefficients.

Figure 2(b) shows the SPDs of the tunable LED light source with 11 LED channels at the maximum intensities measured with Konia Minolta spectroradiometer CS-1000. Out of these 11 LED channels, 3 channels had a broad-band white light source with a correlated color temperature of 3000, 4000, and 4500 kelvins. The remaining 8 LED channels showed a narrow-band light source. The SPD samples with independent control of driver current of each channel at the step of 10% were measured. It is shown that the spectra peak wavelengths shift with the drive currents for some channels, especially for the 4th channel, of which the peak wavelength shifts over 8 nm, as illustrated in Fig. 2(c). Therefore, the measured SPD samples along with the cubic spline interpolation were applied to predict the SPD of the 2nd channel, the 4th channel, the 5th channel, the 8th channel, the 9th channel, and the 10th channel, with peak wavelength shifting 4 nm, 8 nm, 5 nm, 3 nm, 3 nm, and 4 nm, respectively. Specifically, the subroutine *spline* from MATLAB was used to model the LED SPD for the arbitrary weight coefficient from the measured SPDs for the two neighbouring weight coefficients. Then, the predicted SPDs can be used to construct the synthesized SPD according to Eq. (3).

4.2. Simulated experiments

In simulated experiments, we estimated spectral reflectances of Munsell matte color chart with 1269 color patches [40], SFU dataset with 1995 surfaces collated at the Simon Fraser University [41], and TC3.5 CMYK color chart with 540 color patches, using three SPD optimization described in Section 3 and nine spectral estimation algorithms.

The camera responses of Munsell, SFU and TC3.5 datasets were simulated using reflectance data, the Nikon D200 camera sensitivities and the LED SPDs based on the mathematical model as Eq. (2). Reflectance data of TC3.5 color patches was measured with X-Rite I1. Then, reflectance values ranging from 400 to 700 nm at 10-nm intervals were extracted.

Munsell, SFU and TC3.5 datasets were respectively divided into three sets: training set, validation set, and target set. The odd samples were used as training samples; the odd ones of the even samples were used as validation samples; and others were target samples. Validation set was used to determine the RLS [12], RLLM [13], Kernel [14], LLR [16], and SWNR [17] algorithm parameters. Utilizing the SPD optimization methods described in Section 3, optimized SPDs were calculated for the three sets of target samples. Spectral reflectances of the target samples were estimated using these optimized SPDs and various spectral estimation algorithms.

To validate the spectral estimation performances under the best SPDs among three optimization algorithms, the spectral reflectances of three target sets under CIE standard illuminants D65, D50, A and the three white LEDs from LEDCube were also be estimated. In this work, the SPDs of D65, D50 and A light sources from VeriVide light cabinet were measured with Konia Minolta spectroradiometer CS-1000 to compare the results with the following real experiment results. The spectral estimation accuracy was evaluated by relative absolute error (*RAE*) as Eq. (14), which was the same as that used in NTIRE 2018 and NTIRE 2020 challenge on spectral reconstruction.

$$RAE = |\hat{\mathbf{r}}_i - \mathbf{r}_i|/\mathbf{r}_i, \tag{14}$$

where $\hat{\mathbf{r}}_i$ and $\mathbf{r}_i$ denote the estimated and actual spectral reflectance of the *i*th target sample, respectively.

4.3. Real experiments

The real experiments were carried out using the optimized lights generated by LEDCube from a light cabinet, whose intensity of each channel was adjusted according to the above optimized weight coefficient, D65, D50 and A light sources from VeriVide light cabinet, and three white LEDs of LEDCube. The Nikon D200 camera was used to capture the images of TC3.5 CMYK color chart and gray board (whose raw RGB data was used to correct lighting uniformity [11]). The exposure time and f-number were carefully set to acquire the maximum unclipped camera

responses for white patches, with ISO set to 100. The raw 'NEF' format files from the camera were converted to 'tiff' format files by the software dcraw. The 'tiff' format files were de-mosaiced using MATLAB's built-in de-mosaicing algorithm. The average raw camera response values of the areas about 40×40 pixels corresponding to the spectrophotometer X-Rite I1 (which was used to measure the reflectances of TC3.5 color patches in previous experiments) aperture area were extracted. The spectral estimation accuracy of different light sources was also evaluated by *RAE*.

5. Results and discussion

In this section, the three SPD optimization methods are compared with each other. Then, the superiority of the optimized SPDs over common white lights is validated. Moreover, the effect of camera spectral sensitivities and testing samples on optimized SPDs are also discussed.

5.1. Performances of different optimization methods

The mean and maximum spectral estimation results of three optimization algorithms with nine spectral estimation methods are calculated and summarized in Table 1. The best results among three optimization methods are reported in bold font. It is can be seen from Table 1 that, for three testing sets, the optimized SPDs by MPGA almost always give the best spectral recovery; meanwhile, the optimized SPDs by PSO come second, and the optimized SPDs by MC are the worst.

Table 1. Comparison of performances of the three SPD optimization methods along with the nine spectral estimation algorithms for the Munsell, SFU and TC3.5 datasets

Algorithm	RAE (%)	Munsell matte			SFU			TC3.5 CMYK		
		MC	PSO	MPGA	MC	PSO	MPGA	MC	PSO	MPGA
PI	Mean	7.33	7.12	**6.89**	9.25	9.15	**8.91**	7.82	7.30	**7.02**
	Max	48.63	48.14	**41.36**	52.57	**47.89**	50.60	59.89	**41.32**	42.92
RLS	Mean	4.75	4.75	**4.58**	8.22	8.13	**8.03**	3.17	2.92	**2.87**
	Max	40.62	41.30	**36.00**	51.90	**50.67**	51.12	56.20	**53.33**	54.61
RLLM	Mean	4.41	4.33	**4.23**	7.80	**7.62**	7.63	3.52	3.17	**3.07**
	Max	43.89	44.75	**42.32**	53.30	40.39	**40.01**	49.75	38.49	**36.33**
RBF	Mean	4.79	**4.34**	4.41	8.42	8.07	**8.00**	2.99	2.90	**2.81**
	Max	45.83	41.36	**40.29**	**39.46**	42.40	41.92	45.37	**34.90**	40.60
Kernel	Mean	4.38	4.16	**4.10**	8.22	8.00	**7.98**	3.22	2.95	**2.82**
	Max	44.09	40.89	**35.74**	45.44	43.38	**43.30**	47.75	50.27	48.32
WNR	Mean	4.41	4.33	**4.09**	7.73	**7.53**	7.53	3.19	2.90	**2.80**
	Max	43.20	43.37	**37.74**	44.32	**43.30**	43.55	44.43	41.56	**40.78**
LLR	Mean	4.18	**3.99**	3.99	7.71	**7.51**	7.51	3.40	2.90	**2.89**
	Max	43.12	**40.34**	41.10	43.61	41.46	**41.19**	52.33	42.46	**41.28**
SRR	Mean	7.96	**7.76**	7.83	9.22	8.91	**8.68**	14.79	11.62	**11.23**
	Max	37.94	40.95	**35.95**	46.65	48.33	48.24	56.25	39.67	**39.23**
SWNR	Mean	3.97	3.77	**3.76**	7.28	7.16	**6.98**	3.12	2.77	**2.71**
	Max	43.21	38.49	**38.05**	50.38	54.12	**47.54**	59.28	**40.13**	43.01

To assess whether the differences of spectra estimated with three optimized SPDs are statistically significant, a nonparametric test Wilcoxon sign test (WST) is used to compare the whole spectral error distributions. All the pairwise comparisons between SPD optimization methods based on nine spectral estimation methods for three testing sets are done with a significance level $p = 0.05$.

The *p*-values reported in Table 2 indicate the statistical significance. For each spectral estimation method and each testing set, the bold *p*-values in Table 2 indicate rejection of the null hypothesis. It is clear that: the performance of MPGA is significantly better than PSO for most spectral estimation algorithms except for RBF, LLR and SWNR in Munsell dataset; the superiority of MPGA over PSO is significant for PI, RLS, LLR, SSR but insignificant for RLLM, RBF, Kernel, WNR, SWNR in SFU dataset; the differences between MPGA and PSO for all the spectral estimation algorithms except for LLR are significant in TC3.5 dataset; meanwhile, the superiority of MPGA and PSO over MC is significant for almost every spectral estimation algorithm.

Table 2. Comparison of the whole spectral error distributions of the three SPD optimization methods along with the nine spectral estimation algorithms for the Munsell, SFU and TC3.5 datasets

Method		Munsell matte		SFU		TC3.5 CMYK	
		MC	PSO	MC	PSO	MC	PSO
PI	PSO	**0.000**	-	**0.038**	**-**	**0.000**	-
	MPGA	**0.000**	**0.000**	**0.000**	**0.000**	**0.000**	**0.000**
RLS	PSO	0.199	-	**0.000**	**-**	**0.000**	-
	MPGA	**0.000**	**0.000**	**0.000**	**0.028**	**0.000**	**0.000**
RLLM	PSO	**0.000**	-	0.588	-	**0.000**	-
	MPGA	**0.000**	**0.001**	0.598	0.381	**0.000**	**0.001**
RBF	PSO	**0.001**	-	**0.000**	**-**	0.327	-
	MPGA	**0.002**	0.483	**0.000**	0.829	**0.000**	**0.016**
Kernel	PSO	**0.000**	-	**0.001**	**-**	**0.000**	-
	MPGA	**0.000**	**0.037**	**0.003**	0.496	**0.000**	**0.047**
WNR	PSO	**0.000**	-	**0.008**	**-**	**0.000**	-
	MPGA	**0.000**	**0.000**	**0.000**	0.367	**0.000**	**0.000**
LLR	PSO	**0.000**	-	**0.000**	**-**	**0.000**	-
	MPGA	**0.000**	0.699	**0.000**	**0.044**	**0.000**	0.371
SRR	PSO	**0.000**	-	**0.000**	**-**	**0.000**	-
	MPGA	**0.017**	**0.000**	**0.000**	**0.000**	**0.000**	**0.000**
SWNR	PSO	**0.000**	-	**0.000**	**-**	0.094	-
	MPGA	**0.000**	0.921	**0.000**	0.116	**0.010**	**0.000**

The optimized SPDs using MPGA with nine spectral estimation methods are plotted in Fig. 3. It can be seen that the optimized SPDs show stronger intensities at 420 nm, 640 nm or 660 nm wavelength.

5.2. Validation of optimized SPDs

For validating the optimized SPDs by MPGA, based on simulated camera responses from Nikon D200 camera, and D65, D50, A and three white LED light sources (LED (4000 K), LED (4500 K), LED (3000 K)), spectral reflectances of Munsell, SFU and TC3.5 target samples were estimated as well. Furthermore, to check the performance of optimized SPDs in practice, spectral refelctances of TC3.5 target color patches under different light sources were estimated.

Table 3, Table 4, Table 5 and Table 6 summarize the mean and maximum spectral error *RAE*s between the measured and estimated spectral reflectance under the two experiment conditions. The best result of each row is reported in bold font. As can be seen, the optimized SPDs result in the smallest spectral error compared to standard light sources and white LED light sources whether based on simulated or real camera responses. Meanwhile, it is noticed that the whole spectral errors from real camera responses are bigger than those from simulated camera responses,
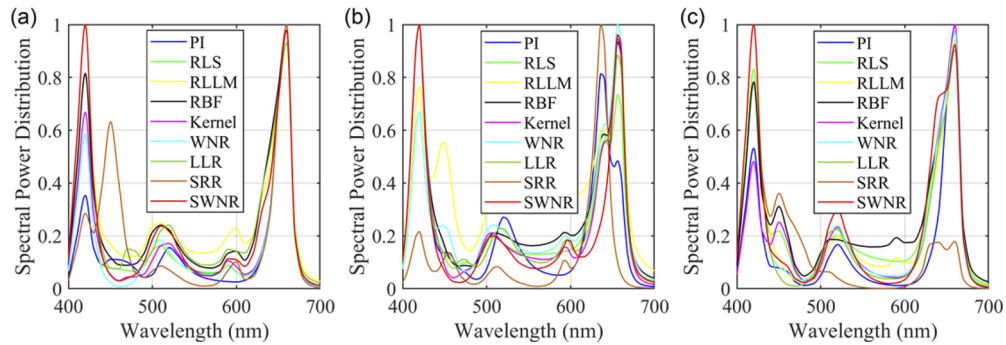
Fig. 3. The optimized SPDs for three target sets using MPGA: (a) Munsell matte, (b) SFU, and (c) TC3.5 CMYK.

which may be attributed to two factors: errors between predicted and real camera noises, and incomplete alignment for areas of reflectance measurement and raw RGBs extraction.

Table 3. Comparison of performances of different SPDs for the Munsell color patches based on simulated camera responses

Testing set	Method	RAE (%)	D65	D50	A	LED (4000 K)	LED (4500 K)	LED (3000 K)	Optimized SPD
Munsell matte	PI	Mean	8.10	8.25	8.02	12.32	8.53	8.16	**6.89**
		Max	64.51	66.98	60.31	71.52	69.60	65.33	**41.36**
	RLS	Mean	5.83	5.97	5.68	10.38	6.36	5.88	**4.58**
		Max	<u>54.76</u>	57.39	49.89	62.13	<u>60.03</u>	55.61	**36.00**
	RLLM	Mean	5.38	5.45	5.14	10.20	5.80	5.35	**4.23**
		Max	55.52	59.23	<u>46.35</u>	62.63	62.33	55.51	**42.32**
	RBF	Mean	5.64	5.75	5.41	9.96	5.93	5.46	**4.41**
		Max	55.74	<u>57.08</u>	48.85	<u>60.10</u>	60.87	54.93	**40.29**
	Kernel	Mean	5.45	5.52	5.18	10.24	5.85	5.34	**4.10**
		Max	55.47	58.02	47.41	60.91	61.49	<u>54.18</u>	<u>**35.74**</u>
	WNR	Mean	5.51	5.59	5.21	9.94	5.91	5.37	**4.09**
		Max	55.84	59.02	48.31	61.00	62.49	55.69	**37.74**
	LLR	Mean	4.98	5.14	5.09	10.27	5.43	5.18	**3.99**
		Max	55.55	58.58	50.66	66.28	62.00	56.62	**41.10**
	SRR	Mean	8.88	9.03	9.23	14.98	9.51	9.26	**7.83**
		Max	60.04	63.76	51.72	70.89	68.05	60.24	**35.95**
	SWNR	Mean	<u>4.92</u>	<u>4.95</u>	<u>4.75</u>	<u>9.72</u>	<u>5.22</u>	<u>4.85</u>	<u>**3.76**</u>
		Max	55.90	58.21	48.99	72.80	61.83	55.29	**38.05**

Spectral error differences between spectra estimated from the optimized SPDs and common light sources were compared with WST statistical analysis. For Munsell and SFU datasets, all the *p*-values between pairwise light sources are smaller than 0.05, so there are significant differences between the optimized SPDs and common light sources in spectral error for these two datasets; however, for TC3.5 dataset, some *p*-values between pairwise light sources are larger than 0.05, and the results are shown in Table 7. The bold *p*-values mean significant differences between pairwise light sources. Specifically, when some spectral estimation methods including Kernel ($p = 0.504$), WNR ($p = 0.387$), LLR ($p = 0.225$), SRR ($p = 0.242$) and SWNR ($p = 0.124$) are

Table 4. Comparison of performances of different SPDs for the SFU dataset based on simulated camera responses

Testing set	Method	RAE (%)	D65	D50	A	LED (4000 K)	LED (4500 K)	LED (3000 K)	Optimized SPD
SFU	PI	Mean	10.20	10.36	10.38	16.56	10.55	10.34	**8.91**
		Max	60.88	63.86	59.26	206.77	66.43	62.63	**50.60**
	RLS	Mean	9.13	9.28	9.28	14.39	9.46	9.19	**8.03**
		Max	57.76	58.98	64.88	106.05	79.95	67.94	**51.12**
	RLLM	Mean	8.63	8.66	8.83	14.47	8.76	8.70	**7.63**
		Max	97.20	103.15	52.55	124.01	118.80	51.64	**40.01**
	RBF	Mean	9.27	9.30	9.61	14.54	9.42	9.24	**8.00**
		Max	57.72	57.57	82.30	85.24	66.41	64.31	**41.92**
	Kernel	Mean	8.79	8.84	8.88	14.04	8.84	8.71	**7.98**
		Max	83.38	86.20	55.80	104.93	84.00	56.13	**43.30**
	WNR	Mean	8.72	8.75	8.75	14.05	8.74	8.52	**7.53**
		Max	68.90	70.09	54.41	82.91	75.80	50.29	**43.55**
	LLR	Mean	8.42	8.60	8.77	14.64	8.77	8.69	**7.51**
		Max	59.45	62.10	55.32	109.79	74.27	54.93	**41.19**
	SRR	Mean	10.10	10.30	10.76	19.14	10.42	10.58	**8.68**
		Max	55.00	59.29	49.65	141.61	63.09	56.46	**48.24**
	SWNR	Mean	8.06	8.17	8.20	13.80	8.35	8.10	**6.98**
		Max	61.73	61.78	56.71	74.34	71.14	56.21	**47.54**

Table 5. Comparison of performances of different light sources for the TC3.5 color patches based on simulated camera responses

Testing set	Method	RAE (%)	D65	D50	A	LED (4000 K)	LED (4500 K)	LED (3000 K)	Optimized SPD
TC3.5 CMYK	PI	Mean	9.07	9.35	9.40	19.19	9.78	9.63	**7.02**
		Max	73.50	83.77	129.18	742.09	93.76	129.10	**42.92**
	RLS	Mean	4.07	4.04	4.19	9.51	4.43	4.16	**2.87**
		Max	68.77	77.20	119.73	197.85	101.99	122.89	**54.61**
	RLLM	Mean	4.52	4.55	3.87	10.01	5.03	4.45	**3.07**
		Max	52.21	58.95	88.28	97.00	59.85	90.09	**36.33**
	RBF	Mean	3.92	3.96	4.06	9.72	4.38	4.14	**2.81**
		Max	51.58	64.97	95.76	153.13	90.67	108.60	**40.60**
	Kernel	Mean	3.94	3.90	3.29	10.80	4.27	4.12	**2.82**
		Max	50.96	54.39	87.42	216.35	64.25	94.40	**48.32**
	WNR	Mean	4.05	3.93	3.25	8.48	4.26	3.93	**2.80**
		Max	68.52	64.49	89.08	56.72	76.53	97.18	**40.78**
	LLR	Mean	4.09	4.08	3.66	12.24	4.41	4.22	**2.89**
		Max	57.77	65.20	87.80	397.43	82.11	100.80	**41.28**
	SRR	Mean	16.32	16.56	17.55	25.51	17.39	17.49	**11.23**
		Max	100.00	100.00	100.00	222.58	100.00	100.00	**39.23**
	SWNR	Mean	3.90	3.80	3.24	8.51	4.31	3.83	**2.71**
		Max	53.93	69.42	88.61	72.90	41.11	52.47	43.01

Table 6. Comparison of performances of different light sources for the TC3.5 color patches based on real camera responses

Testing set	Method	RAE (%)	D65	D50	A	LED (4000 K)	LED (4500 K)	LED (3000 K)	Optimized LED
TC3.5 CMYK	PI	Mean	10.76	11.77	9.91	20.18	11.34	10.64	**8.07**
		Max	149.54	169.99	124.13	284.51	133.07	120.18	**72.56**
	RLS	Mean	4.66	5.75	5.11	11.45	5.79	5.23	**3.49**
		Max	96.15	<u>87.23</u>	156.19	186.73	99.34	152.37	**61.89**
	RLLM	Mean	4.88	5.99	4.43	10.94	5.58	4.99	**3.75**
		Max	78.71	88.09	87.79	186.93	88.56	59.51	**50.50**
	RBF	Mean	4.47	5.89	4.47	10.54	5.82	5.06	**3.48**
		Max	75.12	100.82	87.04	<u>181.43</u>	126.06	66.31	**46.31**
	Kernel	Mean	4.14	5.31	4.08	10.78	4.80	4.24	**3.46**
		Max	92.44	87.89	87.89	188.98	<u>88.14</u>	62.94	**<u>44.09</u>**
	WNR	Mean	4.17	5.24	3.92	10.08	<u>4.71</u>	4.23	**3.42**
		Max	75.39	88.81	92.84	188.93	88.68	74.64	**49.60**
	LLR	Mean	4.46	5.25	4.24	10.30	5.18	4.61	**3.63**
		Max	75.33	87.69	97.97	186.13	88.28	93.66	**50.32**
	SRR	Mean	17.34	18.06	17.88	26.56	18.14	18.15	**12.03**
		Max	139.73	164.86	128.04	287.63	106.57	120.30	**77.67**
	SWNR	Mean	<u>4.01</u>	<u>5.06</u>	<u>3.85</u>	<u>9.67</u>	4.72	<u>4.13</u>	**<u>3.29</u>**
		Max	<u>74.77</u>	88.24	<u>51.50</u>	187.87	88.86	<u>50.46</u>	**47.29**

used in simulation, the differences of spectra errors between optimized SPDs and SPDs from A are not significant; when some spectral estimation methods including RBF ($p = 0.050$), Kernel ($p = 0.231$), WNR ($p = 0.135$), LLR ($p = 0.278$) and SWNR ($p = 0.180$) are used in practice, the superiority of optimized SPDs over D65 or A light source is also not significant. As a whole, optimized light sources can give better spectral estimation to varying degrees than other light sources.

5.3. Performances of different spectral estimation methods

In Table 3, Table 4, Table 5 and Table 6, the smallest mean and maximum *RAEs* of each column are underlined. They indicate that for almost all cases, SWNR can recover spectral reflectance with a higher or similar accuracy than other methods considered. WST statistical analysis of the whole spectral error distribution differences between SWNR and other methods with optimized SPDs is also performed, and the results are shown in Table 8. The bold *p*-values mean significant differences between pairwise spectral estimation methods. It can be seen that the superiority of SWNR varies from testing sets when optimized SPDs are used. Specifically, for simulated RGBs of Munsell dataset, SWNR performs significantly better than other methods except for LLR; for simulated RGBs of SFU dataset, SWNR always performs significantly better than other methods; for simulated and real RGBs of TC3.5 color patches, the superiority of SWNR over PI, RLLM, LLR, SRR is significant, but the differences between SWNR and RLS, RBF, Kernel, WNR are not significant.

5.4. Color fidelity of optimized SPDs and SWNR

In Table 9 and Table 10, the statistical results of reflectance estimation using SWNR and optimized SPDs in ΔE_{ab}^* (D65/10°) are presented. The comparison of Table 9 shows that optimized SPDs

Table 7. Comparison of the whole spectral error distributions between optimized SPDs and other light sources

Testing set	Method	D65	D50	A	LED (4000 K)	LED (4500 K)	LED (3000 K)
TC3.5 CMYK (simulated)	PI	**0.000**	**0.000**	**0.000**	**0.000**	**0.000**	**0.000**
	RLS	**0.000**	**0.000**	**0.000**	**0.000**	**0.000**	**0.000**
	RLLM	**0.000**	**0.000**	0.002	**0.000**	**0.000**	**0.000**
	RBF	**0.000**	**0.000**	**0.000**	**0.000**	**0.000**	**0.000**
	Kernel	**0.000**	**0.000**	0.504	**0.000**	**0.000**	**0.000**
	WNR	**0.000**	**0.000**	0.387	**0.000**	**0.000**	**0.000**
	LLR	**0.000**	**0.000**	0.225	**0.000**	**0.000**	**0.000**
	SRR	**0.000**	**0.000**	0.242	**0.000**	**0.000**	**0.000**
	SWNR	**0.000**	**0.000**	0.124	**0.000**	**0.000**	**0.000**
TC3.5 CMYK (real)	PI	**0.000**	**0.000**	**0.000**	**0.000**	**0.000**	**0.000**
	RLS	**0.000**	**0.000**	0.036	**0.000**	**0.000**	**0.000**
	RLLM	**0.010**	**0.000**	**0.000**	**0.000**	**0.000**	**0.000**
	RBF	0.050	**0.000**	**0.000**	**0.000**	0.001	**0.000**
	Kernel	**0.000**	**0.000**	0.231	**0.000**	0.003	**0.000**
	WNR	0.135	**0.000**	0.009	**0.000**	0.004	**0.000**
	LLR	0.278	**0.000**	0.005	**0.000**	**0.000**	**0.000**
	SRR	**0.000**	**0.000**	**0.000**	**0.000**	**0.000**	**0.000**
	SWNR	0.180	**0.000**	0.004	**0.000**	**0.000**	**0.000**

Table 8. Comparison of the whole spectral error distributions of SWNR and other eight spectral estimation methods with optimized SPDs for the Munsell, SFU and TC3.5 datasets

Testing set	PI	RLS	RLLM	RBF	Kernel	WNR	LLR	SRR
Munsell matte (simulated)	**0.000**	**0.000**	**0.000**	**0.000**	**0.000**	**0.000**	0.080	**0.000**
SFU (simulated)	**0.000**	**0.000**	**0.000**	**0.000**	**0.000**	**0.000**	**0.000**	**0.000**
TC3.5 CMYK (simulated)	**0.000**	0.290	**0.000**	0.210	0.289	0.845	**0.014**	**0.000**
TC3.5 CMYK (real)	**0.000**	0.696	**0.000**	1.000	0.237	0.413	**0.003**	**0.000**

can generate higher accuracy for Munsell and TC3.5 datasets than common light sources, but comparable accuracy for SFU dataset to D65 light source. Furthermore, the results with WST statistical analysis show that there are significant differences between the optimized SPDs and common light sources in ΔE_{ab}^{*} for all datasets, with exceptions that the optimized light source can not give much better results than D65 ($p = 0.722$) and A ($p = 0.085$) light sources for TC3.5 dataset in reality. The comparison of Table 10 shows that SWNR gives similar results to some spectral estimations like LLR or WNR for Munsell and TC3.5 datasets in simulation, and even worse results than some spectral estimations including RLLM, RLS, RBF, Kernel, WNR and LLR for SFU dataset in simulation. However, SWNR always performs better than other spectral estimations for TC3.5 dataset in reality. Meanwhile, the results with WST statistical analysis show that the superiority of SWNR is always significant for TC3.5 dataset in reality.

5.5. Correlation between optimized SPDs and other imaging conditions

For a more in-depth analysis into optimized SPDs, we investigated the effect of camera spectral sensitivities and testing samples on optimized SPDs.

In addition to the Nikon D200 camera we used camera spectral sensitivities from other two cameras to calculate the optimized light source SPDs of TC 3.5 CMYK target set using the

Table 9. Comparison of performances of different light sources in $\Delta E_{ab}{}^*$ for reflectance estimation using SWNR

Testing set	$\Delta E_{ab}{}^*$	D65	D50	A	LED (4000 K)	LED (4500 K)	LED (3000 K)	Optimized SPD
Munsell matte (simulated)	Mean	2.40	2.57	2.89	7.32	2.53	2.74	**1.99**
	Max	9.14	11.97	14.70	31.67	9.81	12.71	**6.43**
SFU (simulated)	Mean	**2.85**	3.06	3.86	8.60	2.94	3.40	2.86
	Max	**15.33**	19.99	31.86	66.59	15.94	20.22	25.52
TC3.5 CMYK (simulated)	Mean	2.34	2.42	2.38	9.22	2.72	2.95	**1.76**
	Max	10.83	11.73	15.44	51.74	17.74	14.26	**7.37**
TC3.5 CMYK (real)	Mean	1.41	1.71	1.31	4.13	1.56	3.17	**1.28**
	Max	23.87	32.54	32.77	35.25	32.97	26.62	**5.67**

Table 10. Comparison of performances of different spectral estimation methods in $\Delta E_{ab}{}^*$ for reflectance estimation using optimized light sources

Testing set	$\Delta E_{ab}{}^*$	PI	RLS	RLLM	RBF	Kernel	WNR	LLR	SRR	SWNR
Munsell matte (simulated)	Mean	3.32	2.10	2.03	1.97	2.02	2.14	**1.92**	3.90	1.99
	Max	22.77	12.02	**5.63**	8.43	9.56	13.13	6.63	10.52	6.43
SFU (simulated)	Mean	4.15	2.79	**2.49**	2.65	2.75	2.54	2.69	3.29	2.86
	Max	32.45	15.72	16.53	11.93	20.31	14.17	15.87	**10.35**	25.52
TC3.5 CMYK (simulated)	Mean	5.13	2.01	1.93	1.98	1.95	**1.73**	1.92	8.42	1.76
	Max	18.04	9.02	9.96	**6.50**	7.29	7.90	9.51	24.74	7.37
TC3.5 CMYK (real)	Mean	4.43	2.55	2.28	2.33	2.14	2.10	2.27	8.08	**1.28**
	Max	13.82	11.26	12.42	9.48	8.26	12.80	9.20	21.18	**5.67**

MPGA optimization method together with SWNR spectral estimation model. The two cameras were Canon D60 and Sony NEX 5N. Figure 4 shows the spectral sensitivity functions of the Nikon D200 camera measured by Sole et al. [37] and those of the two cameras measured by Jiang et al. [42]. After adding the same noises as Nikon D200's to the ideal camera responses, the optimized SPDs for all cameras used to estimate TC3.5 target samples are calculated and plotted in Fig. 5(a). Then, training set and validation set were kept the same, but target samples were replaced by 24 samples from ColorChecker Passport. The optimized SPD for each sample is shown in Fig. 5(b). From Fig. 5(a) we observe that all the optimized lights have the highest relative power distributions at short or long wavelengths and lower relative power distributions at middle wavelengths, but the relative values at short and middle wavelengths for different cameras are different to some extent; From Fig. 5(b) it is seen that optimized SPDs of most of samples have highest intensities at short or long wavelengths but those of two samples have highest intensities at middle wavelengths.

For each camera, **M** in Eq. (2), denoting camera spectral sensitivities weighted by the optimized SPD, is calculated. Then, the weighted camera spectral sensitivities are illustrated in Fig. (6). It can be observed from Figs. 6(a), (b), (c) that, compared to the original camera spectral sensitivities showed in Figs. 4(a), (b), (c), the weighted camera spectral sensitivities have lower overlaps. These results are in line with previous findings in [43]. As declared in [43], 'algebraically, spreading with low overlap means orthogonality', which means that weighted camera spectral sensitivities are much closer to orthogonality with each other. When weighted camera spectral sensitivities are mutually orthogonal, noise cannot affect synergistically on three channels [43], which results in that weighted camera spectral sensitivities tend to span the spectral reflectance subspace. That is to say, optimized SPDs make weighted camera spectral sensitivities more
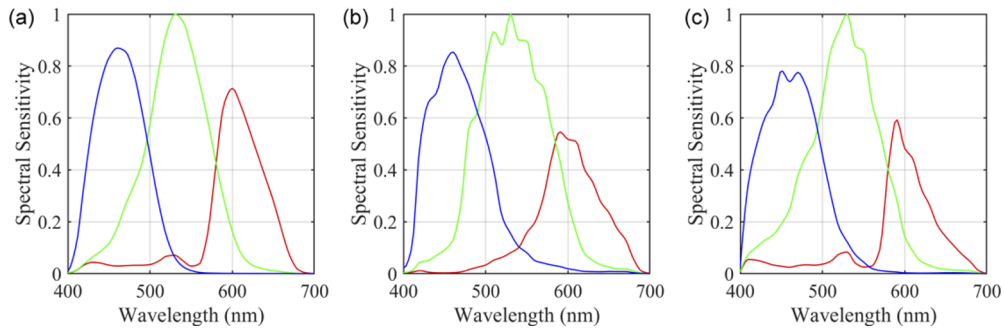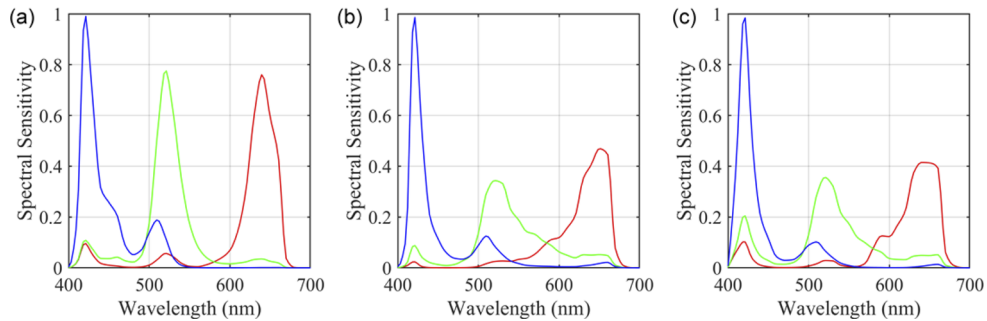
Fig. 4. (a) The spectral sensitivities of the Nikon D200, (b) the spectral sensitivities of the Canon D60, and (c) the spectral sensitivities of the Sony NEX 5N.
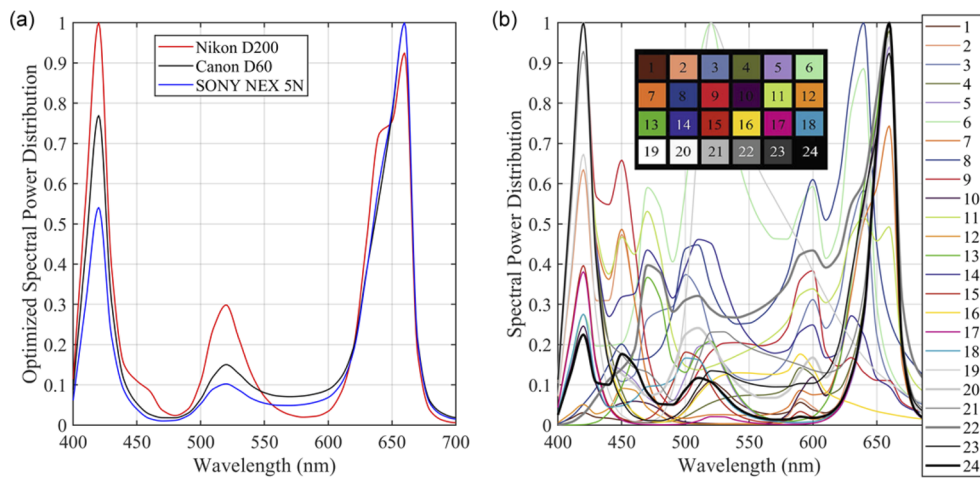
Fig. 5. (a) The optimized SPDs for the TC3.5 color patches using different camera sensitivities, and (b) the optimized SPD for each color patch from ColorChecker Passport using Nikon D200

separate to reduce the effect of noise on camera responses, then weighted camera spectral sensitivities can span the spectral reflectance subspace, and the performance of spectral recovery is improved finally.

Fig. 6. (a) The weighted spectral sensitivities of the Nikon D200, (b) the weighted spectral sensitivities of the Canon D60, and (c) the weighted spectral sensitivities of the Sony NEX 5N

The spectral estimation performances of 24 color patches using corresponding optimized SPD for each sample are compared with those using one optimized SPD from this target set. Then, it is found that for each sample, its own optimized SPD always give better result, which further indicate that different samples need different optimized SPDs.

6.   Conclusion

Light source SPD plays an important role in spectral recovery from one-shot camera responses. In this paper, seeking the optimal light source SPD was converted to an optimization issue. We used MC, PSO and MPGA based optimization techniques along with PI, RLS [12], RLLM [13], Kernel [14], RBF [29], WNR [15], LLR [16], SRR [28] and SWNR [17] estimation algorithms for optimizing a tunable LED light source SPD to improve the accuracy of estimating the spectral reflectance of an object surface.

The SPDs optimized by the MPGA method produce better spectral recovery than the MC and PSO method. Besides, we find that the spectral errors and colorimetric errors between the measured and estimated spectral reflectance are lower when using the optimized light source SPD compared to the standard illuminants and common white LED light sources. To our knowledge, LEDs show a remarkable superiority to conventional light sources in terms of power adjustability, chromaticity control and luminous efficiency. However, in this multispectral imaging task, it is not true that any LED can give better spectral recovery than conventional light sources, which is proved by the results showed in Table 3, Table 4, Table 5, Table 6 and Table 9 that LED (4000K) performed much worse than three conventional light sources. The reason is that SPDs rather than the types of light sources have great influence on reflectance recovery.

We used nine different estimation algorithms to optimize the light source SPDs and estimate the object surface spectral reflectance. In comparison with the commonly used PI estimation [11,19] and the other spectral estimation algorithms used in this paper, the spectral reflectance estimated by the SWNR model with optimized SPDs is more accurate, though in some cases the superiority of SWNR over RLS, Kernel, WNR and LLR is not very significant. In regards to color accuracy, SWNR can also give comparable or better results when training and testing sets have one kind of material. However, it is worth noting that SWNR using optimized SPDs in color fidelity can not perform better than some spectral methods for dataset with mixed materials.

We used the camera spectral sensitivities of three different digital cameras and 24 target samples to investigate the impact of camera spectral sensitivities and targeting samples on calculating the optimized SPDs. The results show that the optimized SPDs vary with camera spectral sensitivities and target samples. However, in general, light sources whose SPDs mainly focus at long wavelength bands or at short wavelength bands are more appropriate to conduct multispectral imaging based on RGB camera responses. The reason is that optimized SPDs with high intensities at the extremes and low intensities in the middle make camera spectral sensitivities weighted by light source SPD orthogonal and reduce the influence of noise on spectral recovery.

It should be noted that the optimized SPDs are limited by the number of channels and the peak wavelength of each channel. With more advanced tunable LEDs developed, the spectral recovery performance may be improved in the future. Moreover, the sets of training and target samples considered here have limited sizes. The performance of optimized SPDs for deep learning based spectral recovery methods needs further investigation.

Disclosures. The authors declare that there are no conflicts of interest related to this article.

Data availability. Data underlying the results presented in this paper are not publicly available at this time but may be obtained from the authors upon reasonable request.

References
1. A. Pelagotti, A. D. Mastio, A. D. Rosa, and A. Piva, "Multispectral imaging of paintings," IEEE Signal Process. Mag. **25**(4), 27–36 (2008).

2. C. S. Chane, A. Mansouri, F. S. Marzani, and F. Boochs, "Integration of 3D and multispectral data for cultural heritage applications: survey and perspectives," Image Vis. Comput. **31**(1), 91–102 (2013).
3. M. Vilaseca, R. Mercadal, J. Pujol, M. Arjona, M. de Lasarte, R. Huertas, M. Melgosa, and F. H. Imai, "Characterization of the human iris spectral reflectance with a multispectral imaging system," Appl. Opt. **47**(30), 5622–5645 (2008).
4. P. Yuen and M. Richardson, "An introduction to hyperspectral imaging and its application for security, surveillance and target acquisition," Imaging Sci. J. **58**(5), 241–253 (2010).
5. B. Bastani and B. Funt, "Geodesic based ink separation for spectral printing," in *Proceedings of the 16th Color Imaging Conference* (Society for Imaging Science and Technology, 2008), pp. 67–72.
6. E. M. Valero, Y. Hu, J. Hernández-Andrés, T. Eckhard, J. L. Nieves, J. Romero, M. Schnitzlein, and D. Nowack, "Comparative performance analysis of spectral estimation algorithms and computational optimization of a multispectral imaging system for print inspection," Color Res. Appl. **41**(6), 585–595 (2016).
7. Q. Li, X. He, Y. Wang, H. Liu, D. Xu, and F. Guo, "Review of spectral imaging technology in biomedical engineering achievements and challenges," J. Biomed. Opt. **18**(10), 100901 (2013).
8. L. Gao, R. T. Kester, and T. S. Tkaczyk, "Compact image slicing spectrometer (ISS) for hyperspectral fluorescence microscopy," Opt. Express **17**(15), 12293–12308 (2009).
9. J. P. Kerekes and J. R. Schott, Hyperspectral Data Exploitation: Theory and Applications (Wiley, 2006).
10. S. Tominaga and T. Horiuchi, "Spectral imaging by synchronizing capture and illumination," J. Opt. Soc. Am. A **29**(9), 1764–1775 (2012).
11. X. Zhang, Q. Wang, J. Li, X. Zhou, Y. Yang, and H. Xu, "Estimating spectral reflectance from camera responses based on CIE XYZ tristimulus values under multi-illuminants," Color Res. Appl. **42**(1), 68–77 (2017).
12. V. Heikkinen, T. Jetsu, J. Parkkinen, M. Hauta-Kasari, T. Jaaskelainen, and S. D. Lee, "Regularized learning framework in the estimation of reflectance spectra from camera responses," J. Opt. Soc. Am. A **24**(9), 2673–2683 (2007).
13. W. Zhang, G. Tang, D. Dai, and A. Nehorai, "Estimation of reflectance from camera responses by the regularized local linear model," Opt. Letters **36**(19), 3933–3935 (2011).
14. T. Eckhard, E. M. Valero, J. Hernández-Andrés, and V. Heikkinen, "Evaluating logarithmic kernel for spectral reflectance estimation—effects on model parametrization, training set size, and number of sensor spectral channels," J. Opt. Soc. Am. A **31**(3), 541–549 (2014).
15. M. M. Amiri and M. D. Fairchild, "A strategy toward spectral and colorimetric color reproduction using ordinary digital cameras," Color Res. Appl. **43**(5), 675–684 (2018).
16. J. Liang, K. Xiao, M. R. Pointer, X. Wan, and C. Li, "Spectra estimation from raw camera responses based on adaptive local-weighted linear regression," Opt. Express **27**(4), 5165–5180 (2019).
17. L. Wang, X. Wan, G. Xiao, and J. Liang, "Sequential adaptive estimation for spectral reflectance based on camera responses," Opt. Express **28**(18), 25830–25842 (2020).
18. J. Y. Hardeberg, "Filter selection for multispectral color image acquisition," J. Imaging Sci. Technol. **48**(2), 105–110 (2004).
19. P. Xu and H. Xu, "Filter selection based on representative training samples for multispectral imaging," Optik **127**(20), 9743–9754 (2016).
20. R. Shrestha and J. Y. Hardeberg, "Multispectral imaging using LED illumination and an RGB image," in *21st Color and Imaging Conference* (Society for Imaging Science and Technology, 2013): pp. 8–13.
21. J. Zhang, Y. Meuret, X. Wang, and K. A. G. Smet, "Improved and Robust Spectral Reflectance Estimation," LEUKOS (2020), https://doi.org/10.1080/15502724.2020.1798246.
22. "LEDCube", retrieved on December 19th, 2020, http://www.thouslite.com/PRODUCTS/16.html.
23. H. A. Khan, J. Thomas, J. Y. Hardeberg, and O. Laligant, "Illuminant estimation in multispectral imaging," J. Opt. Soc. Am. A **34**(7), 1085–1098 (2017).
24. F. Ayala, J. F. Echavarri, and P. Renet, "Use of three tristimulus values from surface reflectance spectra to calculate the principal components to reconstruct these spectra by using only three eigenvectors," J. Opt. Soc. Am. A **23**(8), 2020–2026 (2006).
25. V. Heikkinen, A. Mirhashemi, and J. Alho, "Link functions and Matérn kernel in the estimation of reflectance spectra from RGB responses," J. Opt. Soc. Am. A **30**(11), 2444–2454 (2013).
26. P. Morovic and G. D. Finlayson, "Metamer-set-based approach to estimating surface reflectance from camera RGB," J. Opt. Soc. Am. A **23**(8), 1814–1822 (2006).
27. C. Li and M. R. Luo, "The estimation of spectral reflectances using the smoothness constraint condition," in *Proceedings of IS&T/SID Ninth Color Imaging Conference* (Society for Imaging Science and Technology, 2001): pp. 62–67(6).
28. S. A. Burns, "Numerical methods for smoothest reflectance reconstruction," Color Res. Appl. **45**(1), 8–21 (2020).
29. R. M. Nguyen, D. K. Prasad, and M. S. Brown, "Training-based spectral reconstruction from a single RGB image," in *Proceedings of European Conference on Computer Vision* (Springer), 186–201 (2014).
30. B. Arad, O. B-. Shahar, R. Timofte, L. V. Gool, L. Zhang, and M. -H. Yang, "NTIRE 2018 challenge on spectral reconstruction from RGB images," in *Proceedings of IEEE Conference on Computer Vision and Pattern Recognition Workshops* (IEEE, 2018), pp. 1042–1051.

31. B. Arad, R. Timofte, O. B-. Shahar, Y. -T. Lin, and G. D. Finlayson, "NTIRE 2020 challenge on spectral reconstruction from an RGB image," in *Proceedings of IEEE Conference on Computer Vision and Pattern Recognition Workshops* (IEEE, 2020).

32. R. Gan, Z. Guo, J. Lin, M. Zeng, F. Yang, W. Yan, and M. Lin, "The genetic algorithm in the application of the LED light source spectral matching technology," Guangzi Xuebao **43**(7), 730003 (2014).

33. N. Metropolis, A. W. Rosenbluth, M. N. Rosenbluth, and A. H. Teller, "Equation of state calculations by fast computing machines," J. Chem. Phys. **21**(6), 1087–1092 (1953).

34. J. Kennedy and R. Eberhart, "Particle swarm optimization," in *Proceedings of IEEE International Conference on Neural Networks* (IEEE, 1995), pp. 1942–1948.

35. C.-P. Erick, "A survey of parallel genetic algorithms," Reseaux et Systems Repartis **10**(2), 141–171 (1998).

36. A. Chipperfield, P. Fleming, and H. Pohlheim, "Genetic algorithm toolbox for use with MATLAB User's guide, version 1.2," University of Sheffield (2006).

37. A. Sole, I. Farup, and S. Tominaga, "Image based reflectance measurement based on camera spectral sensitivities," in *Proceedings of International Symposium on Electronic Imaging* (Society for Imaging Science and Technology, 2016): pp. 1–8(8).

38. G. E. Healey and R. Kondepudy, "Radiometric CCD camera calibration and noise estimation," IEEE Trans. Pattern Anal. Machine Intell. **16**(3), 267–276 (1994).

39. H. J. Trussell and R. Zhang, "The dominance of Poisson noise in color digital cameras," in *Proceedings of 19th IEEE International Conference on Image Processing* (IEEE, 2012): pp. 329–332.

40. O. Kohonen, J. Parkkinen, and T. Jääskeläinen, "Databases for spectral color science," Color Res. Appl. **31**(5), 381–390 (2006).

41. K. Barnard, L. Martin, B. Funt, and A. Coath, "A data set for color research," Color Res. Appl. **27**(3), 147–151 (2002).

42. J. Jiang, D. Liu, J. Gu, and S. Süsstrunk, "What is the space of spectral sensitivity functions for digital color cameras?" in *Proceedings of the 2013 IEEE Workshop on Applications of Computer Vision* (IEEE, 2013): pp. 168–179.

43. A. M. Nahavandi and M. A. Tehran, "Metric for evaluation of filter efficiency in spectral cameras," Appl. Opt. **55**(32), 9193–9204 (2016).